

Multi-epoch spectro-photometric characterization of the minimoon 2024 PT₅ in the visible and near-infrared

Jin Beniyama^{1,2}, Bryce T. Bolin³, Alexey V. Sergeev^{1,4}, Marco Delbo^{1,5}, Laura-May Abron⁶, Matthew Belyakov⁷, Tomohiko Sekiguchi⁸, Seiko Takagi⁹

¹ Université Côte d’Azur, Observatoire de la Côte d’Azur, CNRS, Laboratoire Lagrange, Bd de l’Observatoire, CS 34229, 06304 Nice Cedex 4, France
e-mail: jbeniyama@oca.eu

² The Department of Earth and Planetary Science, The University of Tokyo, 7-3-1 Hongo, Bunkyo, Tokyo 113-0033, Japan

³ Eureka Scientific, Oakland, CA 94602, U.S.A.

⁴ Institute of Astronomy, V.N. Karazin Kharkiv National University, 35 Sumska Str., Kharkiv 61022, Ukraine

⁵ School of Physics and Astronomy, University of Leicester, Leicester LE1 7RH, UK

⁶ Griffith Observatory, Los Angeles, CA 90027

⁷ Division of Geological and Planetary Sciences, California Institute of Technology, Pasadena, CA 91125, USA

⁸ Asahikawa Campus, Hokkaido University of Education, Hokumon 9, Asahikawa, Hokkaido 070-8621, Japan

⁹ Department of Earth and Planetary Sciences, Faculty of Science, Hokkaido University, Kita-ku, Sapporo, Hokkaido 060-0810, Japan

Received 07 08, 2025

ABSTRACT

Context. 2024 PT₅ is a tiny ($D \leq 10$ m) near-Earth asteroid (NEA) discovered in August 2024. 2024 PT₅ was gravitationally bound to the Earth-Moon system from September to November 2024 and classified as a minimoon. Several quick response observations suggest the lunar ejecta origin of 2024 PT₅, while rotation state and albedo, essential properties to investigate its origin, are not well constrained.

Aims. We aim to characterize the spectro-photometric properties of 2024 PT₅ by ground-based observations to test its taxonomic classification and origin.

Methods. We performed visible to near-infrared multicolor photometry of 2024 PT₅ from data taken using the TriColor CMOS Camera and Spectrograph (TriCCS) on the Seimei 3.8 m telescope during 2025 January 4–10. The Seimei/TriCCS observations of 2024 PT₅ cover phase angles from 14 deg to 27 deg, and were obtained in the g , r , i , and z bands in the Pan-STARRS system. In addition, we analyzed Y , J , H , and K photometry taken with the Multi-Object Spectrograph for Infrared Exploration (MOSFIRE) on the Keck I 10-m telescope taken on 2025 January 16–17.

Results. Our lightcurves show brightness variations over time periods of several tens of minutes. We infer that 2024 PT₅ is in a tumbling state and has a lightcurve amplitude of about 0.3 mag. Visible and near-infrared color indices of 2024 PT₅, $g - r = 0.567 \pm 0.044$, $r - i = 0.155 \pm 0.009$, $r - z = 0.147 \pm 0.066$, $Y - J = 0.557 \pm 0.046$, $J - H = 0.672 \pm 0.078$, and $H - K_s = 0.148 \pm 0.098$, indicate that 2024 PT₅ is an S-complex asteroid, largely consistent with previous observations. Using the H - G model, we derived an absolute magnitude H_{VHG} of 27.72 ± 0.09 and a slope parameter G_V of 0.223 ± 0.073 in V-band. A geometric albedo of 2024 PT₅ is derived to be 0.26 ± 0.07 from the slope of its photometric phase curve. This albedo value is typical of the S- and Q-type NEAs.

Conclusions. Using the albedo and absolute magnitude, the equivalent diameter of 2024 PT₅ is estimated to be 7.4 ± 1.0 m. The color properties of 2024 PT₅ derived from our observations match rock samples taken from the lunar surface, which agrees with previous studies.

Key words. Minor planets, asteroids: general – Minor planets, asteroids: individual: 2024 PT5 – Techniques: photometric

1. Introduction

The natural bodies gravitationally bound to the Earth-Moon system, with the exception of our Moon, are called minimoons.¹ Depending on whether they are bound more than or less than 1 orbital revolution, they are classified as temporally captured orbiters (TCO) or temporally captured flyby (TCF), respectively (e.g., Granvik et al. 2012, 2013; Jedicke et al. 2018). Minimoons have similar heliocentric orbits with the Earth, and have low

Δv . Thus, minimoons are possible targets of spacecraft missions, and their characterization by telescopic observations is essential (Jedicke et al. 2018). Only four minimoons were discovered before August 2024: 1991 VG (de la Fuente Marcos & de la Fuente Marcos 2018), 2006 RH₁₂₀ (Kwiatkowski et al. 2009), 2020 CD₃ (Bolin et al. 2020; Fedorets et al. 2020b; de la Fuente Marcos & de la Fuente Marcos 2020; Naidu et al. 2021), and 2022 NX₁ (de la Fuente Marcos et al. 2023). Dynamical studies have shown that lunar impacts can produce objects on Earth co-orbital orbits (Gladman et al. 1995; Jedicke et al. 2025). Observational studies of minimoons and Earth co-orbitals in visible to near-infrared light support the possibility that some asteroids originate as lu-

¹ In this paper, we follow the definition by, for example, Kary & Dones (1996); Granvik et al. (2012); de la Fuente Marcos et al. (2025): geocentric energy is smaller than zero, and the geocentric distance is less than three Hill radii of Earth, ~ 0.03 au.

nar ejecta by showing spectral similarity with lunar rock samples (Bolin et al. 2020; Sharkey et al. 2021; Bolin et al. 2025a).

The target of this paper, 2024 PT₅, is the fifth minimoons discovered on 2024 August 7 by the Asteroid Terrestrial-impact Last Alert System in South Africa (Denneau et al. 2024; Bolin et al. 2025a). Soon after the discovery, telescopic observations of 2024 PT₅ have been made worldwide as summarized in Table 1. Fig. 1 shows the predicted magnitude and solar phase angles of 2024 PT₅.

Bolin et al. (2025a) performed visible to near-infrared (0.475 μm to 0.880 μm)² spectrophotometry of 2024 PT₅ using Gemini Multi-Object Spectrograph (GMOS) on Gemini North telescope on 2024 September 27. They found that the spectrum of 2024 PT₅ best matches lunar rock samples followed by S-complex asteroids, making it the third known asteroid with a spectrum similar to lunar rock following 2020 CD₃ and (469219) Kamo'oalewa (Bolin et al. 2020; Sharkey et al. 2021; Bolin et al. 2025a).

Kareta et al. (2025) later reported visible multicolor photometry of 2024 PT₅ using the Lowell Discovery Telescope (LDT) on 2024 August 14. Then they activated target-of-opportunity (ToO) programs of visible and near-infrared spectroscopy of 2024 PT₅ using the LDT and NASA Infrared Telescope Facility on 2024 August 16. Their visible to near-infrared (~ 0.40 μm to 2.45 μm) reflectance spectrum of 2024 PT₅, covering a broad wavelength range, are in agreement with the results of Bolin et al. (2025a), showing that it is compatible with lunar samples.

Additionally, de la Fuente Marcos et al. (2025) characterized 2024 PT₅ using the 10.4 m Gran Telescopio Canarias (GTC), the Two-meter Twin Telescope (TTT), and the Transient Survey Telescope (TST) in the Canary Islands. Three visible to near-infrared (0.480 μm to 0.920 μm) spectra of 2024 PT₅ were obtained using the OSIRIS spectrograph on the GTC on 2024 September 7. Also lightcurve observations of 2024 PT₅ were performed using the GTC/OSIRIS on 2024 September 28. Moreover, the astrometric observations were obtained using the TTT1, TTT2, and the TST. Their visible to near-infrared spectrum are also in agreement with the results of Bolin et al. (2025a), which showed that the visible to near-infrared (0.475 μm to 0.880 μm) spectrum of 2024 PT₅ matches powder samples of a mare breccia of the Moon collected by the Luna 24 mission.

A rotation state of 2024 PT₅ is still unclear though the state-of-the-art ground-based telescopes were used to characterize 2024 PT₅. The rotation state is essential to investigate its origin. For instance, the tumbling state of 2024 PT₅ would support the lunar ejecta origin (Harris 1994). This is because a tumbling motion is a natural outcome after the collisional event. Bolin et al. (2025a) and de la Fuente Marcos et al. (2025) reported that 2024 PT₅ is possibly rotating with a rotation period shorter than ~ 1 hr, while Kareta et al. (2025) concluded that there is no clear periodicity in their lightcurves. Also, the geometric albedo of 2024 PT₅ is not estimated though it is another crucial quantity to investigate the surface property.

In this paper, we report the results of visible multicolor photometry of 2024 PT₅ for one week in 2025 January, when 2024 PT₅ was brighter than 20 mag in visible wavelengths and can be observed in a wide range of phase angles as seen in Fig. 1³. The paper is organized as follows. In Sect. 2, we describe our photometric observations and data reduction with

Seimei/TriColor CMOS Camera and Spectrograph (TriCCS) and Keck/Multi-Object Spectrograph for Infrared Exploration (MOSFIRE). The results of the observations are presented in Sect. 3. The constraints on the physical properties of 2024 PT₅ and its origin are discussed in Sect. 4.

2. Observations and data reduction

We obtained multicolor photometry of 2024 PT₅ in January 2025. The observing conditions are summarized in Table 2. The predicted V-band magnitudes, phase angles, distances between 2024 PT₅ and observer, and distances between 2024 PT₅ and the Sun in Table 2 were obtained from NASA JPL Horizons⁴ using the Python package astroquery (Ginsburg et al. 2019).

2.1. Seimei telescope

We observed 2024 PT₅ using the TriCCS on the 3.8 m Seimei telescope (Kurita et al. 2020) on 2025 January 4, 7, and 10. The telescope is located at the Kyoto University Okayama Observatory (133.5967° E, 34.5769° N, and 355 m in altitude). We simultaneously obtained three-band images in the Pan-STARRS (g , r , i) and (g , r , z) filter (Chambers et al. 2016). The field of view is $12.6' \times 7.5'$ with a pixel scale of 0.350 arcsec pixel⁻¹.

A phase angle of 2024 PT₅ changed from 28.7 deg on 2025 January 4 to 14.3 deg on 2025 January 10. 2024 PT₅ had a geocentric distance of about 0.012 au and a heliocentric distance of about 0.994–0.995 au throughout the observing period. The lunar phases on 2025 January 4, 7, and 10 were ~ 0.2 , ~ 0.6 , and ~ 0.9 , respectively. The lunar elongations on 2024 January 4, 7, and 10 were ~ 120 deg, ~ 80 deg, and ~ 30 deg, respectively. The apparent sky motion of 2024 PT₅ was about 0.13–0.15 arcsec s⁻¹. The seeing measured by using in-field stars was 2.7–3.3 arcsec in the r band.

Non-sidereal tracking was performed during the observations of 2024 PT₅. Exposure times were set to 5 s for all observations. We took multiple images with short exposures rather than a single image with long exposures in our observations to avoid having elongated photometric reference stars and also to eliminate the cosmic rays. We performed standard image reduction, including bias subtraction, dark subtraction, and flat-fielding. The astrometry of reference sources from the Gaia Data Release 2 was performed using the astrometry.net software (Lang et al. 2010).

We performed stacking of images before photometry to increase the signal-to-noise ratio (S/N) of 2024 PT₅ avoiding the elongations of their images as shown in the upper panels of Fig. 2 (hereinafter referred to as the nonsidereally stacked image). The S/N of 2024 PT₅ on the single 5 s images are as low as a few to less than ten. Especially, the S/N of 2024 PT₅ on 2024 January 10 are lower than the others due to the larger lunar phase (~ 0.9) and smaller lunar elongation (~ 30 deg); and the target is barely visible in individual frames. We stacked 20 or 40 successive images with exposure times of 5 s, and obtained images with effective exposure times of 100 s or 200 s. A typical readout time of the CMOS sensors on TriCCS is 0.4 milliseconds, which is negligibly small compared to the exposure time of 5 s. We also stacked images using the World Coordinate System (WCS) of images corrected with the surrounding sources to suppress the elongations of the images of reference stars (hereafter referred to as the sidereally stacked image).

⁴ <https://ssd.jpl.nasa.gov/horizons>

² In this paper, we follow the convention that the boundary between visible and near-infrared wavelengths is set at 0.75 μm (Glass 1999).

³ Kareta et al. (2025) observed 2024 PT₅ at phase angles of ~ 64 deg as written in their main text, not ~ 1 deg as written in their Table 1.

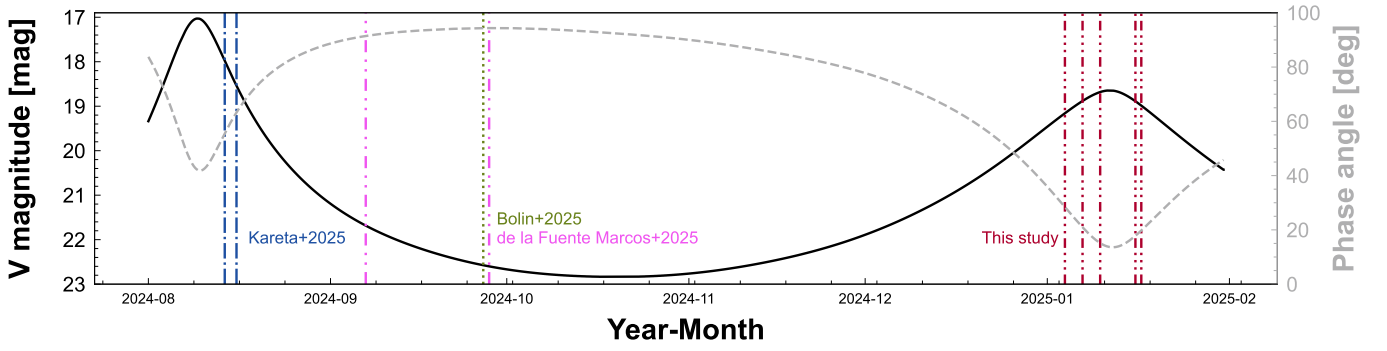


Fig. 1: Predicted magnitude (solid line) and phase angles (dashed line) of 2024 PT₅ obtained from NASA JPL Horizons using the Python package *astroquery* (Ginsburg et al. 2019). Vertical lines show our observations and previous observations: spectrophotometry and spectroscopy in Karetal et al. (2025) (dot-dashed lines), spectroscopy and lightcurve observations in de la Fuente Marcos et al. (2025) (double dot-dashed lines), spectrophotometry in Bolin et al. (2025a) (dotted line), and this study (triple dot-dashed lines).

Table 1: Summary of the existing observations

Reference	Method
Bolin et al. (2025a)	Visible lightcurve (~40 min)
	Spectrophotometry (0.475 μm to 0.880 μm)
Karetal et al. (2025)	Visible lightcurve (~40 min)
	Spectrophotometry & Spectroscopy (~0.40 μm to 2.45 μm)
de la Fuente Marcos et al. (2025)	Visible lightcurve (~1 hr)
	Spectroscopy (0.480 μm to 0.920 μm)

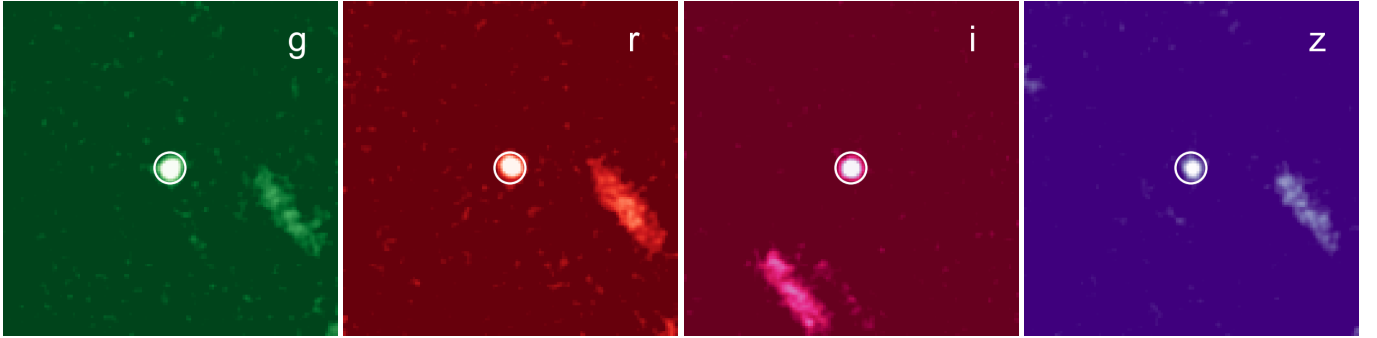


Fig. 2: Non-sidereally stacked images in g , r , i , and z bands with a total integration time of 100 s on 2024 January 4 are shown. Circles indicate 2024 PT₅. Field of view covers 45 $\text{arcsec} \times 45 \text{ arcsec}$. North is to the top and East is to the left.

We derived colors and magnitudes of 2024 PT₅ following the same procedure used in Beniyama et al. (2023c,b,a, 2024). Cosmic rays were removed with the Python package *astroscrappy* (McCully et al. 2018) using the Pieter van Dokkum’s L.A. Cosmic algorithm (van Dokkum 2001). The circular aperture photometry was performed for 2024 PT₅ using the SExtractor-based Python package *sep*. The aperture radii were set to 15 pix, which is about 1.5–2.0 times as large as the FWHMs of the PSFs of the reference stars on the sidereally stacked images, and annuli from 18 to 28 pix from the center were used to estimate the background level and noise for 2024 PT₅. The circular aperture photometry was performed for the reference stars using *sep*, with a circular aperture after global background subtraction. The aperture radii were set to 15 pix as the photometry of 2024 PT₅. The photometric results of 2024 PT₅ and reference stars were obtained from the non-sidereal and sidereal stacked images, respectively.

All images were calibrated using Pan-STARRS catalog Data Release 2 (DR2, Chambers et al. 2016). Reference stars that met

any of the following criteria were excluded from the analysis: uncertainties in the g , r , i , or z band magnitudes in the catalog larger than 0.05 mag; $(g-r)_{\text{PS}} > 1.1$; $(g-r)_{\text{PS}} < 0.0$; $(r-i)_{\text{PS}} > 0.8$; or $(r-i)_{\text{PS}} < 0.0$, where $(g-r)_{\text{PS}}$ and $(r-i)_{\text{PS}}$ are colors in the Pan-STARRS system. Photometric measurements within 100 pixels from the edges of the image or contaminated by nearby sources within the aperture were excluded on a frame-by-frame basis. Extended sources, possible quasars as well as variable stars were removed using *objinfoflag* and *objfilterflag* in the Pan-STARRS catalog. Typically a few dozen of reference stars are used in each frame. When the number of stars in each frame is less than five, we do not use that frame to avoid any systematics in its color and/or magnitude estimates. The typical uncertainties in magnitude zero points are less than 0.01 mag.

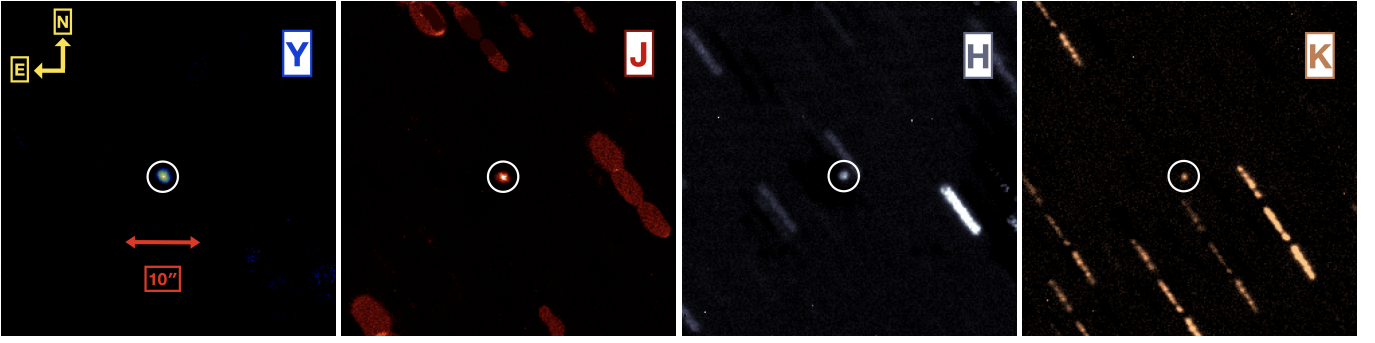


Fig. 3: Non-sidereally stacked images in *Y*, *J*, *H*, and *K* bands with a total integration time of 150 s on 2024 January 16/17 are shown. Circles indicate 2024 PT₅. Field of view covers $45 \text{ arcsec} \times 45 \text{ arcsec}$. North is to the top and East is to the left.

2.2. Keck telescope

Observations of 2024 PT₅ were obtained at the Keck Observatory with the MOSFIRE instrument on the Keck I 10-m telescope on Maunakea on 2025 January 16 under program R332 (PI: Bolin) and N085 (PI: Bolin). MOSFIRE has a $6.12' \times 6.12'$ field of view, plate scale of 0.18 arcsec/pixel, and possesses a *Y* filter (central wavelength $1.048 \mu\text{m}$, FWHM $0.152 \mu\text{m}$), *J* filter (central wavelength $1.253 \mu\text{m}$, FWHM $0.200 \mu\text{m}$), *H* filter (central wavelength $1.637 \mu\text{m}$, FWHM $0.341 \mu\text{m}$), and *K* filter (central wavelength $2.147 \mu\text{m}$, FWHM $0.314 \mu\text{m}$) (McLean et al. 2012).

On 2025 January 16 UTC, 2024 PT₅ had a phase angle of 18.5° , a geocentric distance of 0.013 au, and a heliocentric distance of 0.996 au, and on 2025 January 17, 2024 PT₅ had a phase angle of 20.6° , a geocentric distance of 0.013 au, and a heliocentric distance of 0.996 au. The apparent sky motion of 2024 PT₅ was about $0.12 \text{ arcsec s}^{-1}$. The seeing measured by using in-field stars was $\sim 0.9 \text{ arcsec}$ in the *Y*, *J*, and *H* bands on 2025 January 16 and $\sim 0.6 \text{ arcsec}$ in the *Y* and *K* bands on 2025 January 17. The asteroid was observed in the *Y*, *J*, and *H* filters on 2025 January 16, and in the *Y*, and *K* filters on 2025 January 17 (Fig. 3). Exposure times of 30 s, a five-point dither pattern was used, and the telescope was tracked at the rate of motion of the asteroid. Filters were changed between groups of five exposures between the *Y*, *J*, and *H* filters on 2025 January 16, and between the *Y* and *K* filters on 2025 January 17 to mitigate lightcurve effects on the photometry. Calibration was completed by using in-field solar-like stars from the Pan-STARRS and 2MASS catalogs (Skrutskie et al. 2006; Tonry et al. 2012). Around 10 stars were used per image depending, and catalogue uncertainties for the standard stars in *Y*, *J*, *H*, and *K* bands ranged between 0.02–0.09 mag.

3. Results

3.1. Lightcurves, rotation period, and axial ratio

The lightcurves of 2024 PT₅ are shown in Fig. 4. We see variations with amplitudes of approximately 0.3 mag in all lightcurves. The lightcurves obtained on 2025 January 4 has an observation arc longer than 2 hrs, and the corresponding lightcurve in the *r* band are presented in Figure 5. This is longer than any existing observations (see Table 1).

We performed the periodic analysis with the three *r*-band lightcurves obtained on 2025 January 4 using the Lomb–Scargle technique (Lomb 1976; Scargle 1982; VanderPlas 2018). The Lomb–Scargle periodograms with a period range between 200 s to 8161 s are shown in Fig. 6. We showed 90.0, 99.0, and 99.9%

confidence levels in the periodogram. The minimum and maximum of the period range correspond to twice the sampling rate and observation arc, respectively. We found no periodicity in our lightcurves.

We assumed the asteroid is a triaxial ellipsoid with axial lengths of *A*, *B*, and *C* ($A \geq B \geq C$) and the aspect angle, angle between rotation axis and the asteroids–observer direction, of 90° . A lower limit of axial ratio *A/B* is estimated as follows:

$$A/B \geq 10^{0.4m(\alpha)/(1+s\alpha)}, \quad (1)$$

where $m(\alpha)$ is the lightcurve amplitude at a phase angle of α and s is a slope depending on the taxonomic type of the asteroid (Bowell et al. 1989). When we assume s of 0.030, a typical value of S-type asteroids (Zappala et al. 1990), and a lightcurve amplitude of 0.3, axial ratio *A/B* of 2024 PT₅ is larger than 1.17.

3.2. Colors

The averages and standard deviations of the mean colors of 2024 PT₅ calculated for each observing block were derived as $g - r = 0.567 \pm 0.044$, $r - i = 0.155 \pm 0.009$, and $r - z = 0.147 \pm 0.066$. We summarize the derived colors of 2024 PT₅ and with those reported in previous studies in Table 3. We converted colors from Bolin et al. (2025a) in the SDSS system into the Pan-STARRS system using the following equations (Tonry et al. 2012):

$$g = g_{\text{SDSS}} - 0.012 - 0.139(g_{\text{SDSS}} - r_{\text{SDSS}}), \quad (2)$$

$$r = r_{\text{SDSS}} + 0.000 - 0.007(g_{\text{SDSS}} - r_{\text{SDSS}}), \quad (3)$$

$$i = i_{\text{SDSS}} + 0.004 - 0.014(g_{\text{SDSS}} - r_{\text{SDSS}}), \quad (4)$$

$$z = z_{\text{SDSS}} - 0.013 + 0.039(g_{\text{SDSS}} - r_{\text{SDSS}}), \quad (5)$$

where g , r , i , and z are magnitudes in the Pan-STARRS system, while g_{SDSS} , r_{SDSS} , i_{SDSS} , and z_{SDSS} are magnitudes in the SDSS system. We computed the propagated uncertainties of the colors in the Pan-STARRS system with the photometric errors and uncertainties in conversions. Table 3 also includes colors of Kamo'oalewa from Sharkey et al. (2021) and lunar rock core samples from Isaacson et al. (2011). We used the techniques from Bolin et al. (2021, 2022) to estimate the visible colors in the Pan-STARRS system from spectra. We used the spectroscopy module from sbpy, an astropy-affiliated package for small-body planetary astronomy (Mommert et al. 2019), and solar colors from (Willmer 2018).

We present the derived colors of 2024 PT₅ in Fig. 7 with those of asteroids from the recent catalog (Sergeyev & Carry 2021). In this catalog, the probabilities of the asteroid complex

Table 2: Summary of the observations

	Obs. Date (UTC)	Tel.	Filter	t_{exp} (s)	N_{img}	V (mag)	α (deg)	v (arcsec s ⁻¹)	Air Mass	Seeing (arcsec)
2025 Jan 04	15:23:43–16:02:39	Seimei	g, r, i	100	22	19.1	26.8	0.13	1.04–1.04	2.7
	16:14:35–16:53:00	Seimei	g, r, z	100	19	19.1	26.7	0.14	1.05–1.07	2.8
	17:01:18–17:39:44	Seimei	g, r, i	100	20	19.1	26.7	0.14	1.08–1.13	2.9
2025 Jan 07	16:49:28–17:47:58	Seimei	g, r, i	100	29	18.8	19.4	0.15	1.08–1.20	3.3
2025 Jan 10	15:13:50–16:00:38	Seimei	g, r, z	200	14	18.7	14.4	0.14	1.01–1.05	3.0
	16:07:56–16:54:44	Seimei	g, r, z	200	10	18.7	14.4	0.14	1.06–1.14	3.1
2025 Jan 16	08:44:49–08:47:29	Keck I	Y	30	5	18.9	18.5	0.12	1.01–1.01	0.9
	08:50:56–08:53:53	Keck I	J	30	5	18.9	18.5	0.12	1.00–1.00	0.9
	08:55:33–08:58:17	Keck I	Y	30	5	18.9	18.5	0.12	1.00–1.00	0.9
	08:59:38–09:05:20	Keck I	H	30	5	18.9	18.5	0.12	1.00–1.00	0.9
2025 Jan 17	09:13:43–09:16:26	Keck I	Y	30	5	19.0	20.6	0.12	1.00–1.00	0.6
	09:24:17–09:27:58	Keck I	K	30	5	19.0	20.6	0.12	1.00–1.01	0.6

Notes. Observation time in UT in midtime of exposure (Obs. Date), telescope (Tel.), filters (Filter), total exposure time per frame (t_{exp}), and the number of images (N_{img}) are listed. Predicted V band apparent magnitude (V), phase angle (α), and apparent angular rate of 2024 PT₅ (v) at the observation starting time are referred to NASA Jet Propulsion Laboratory (JPL) Horizons as of July 08, 2025. Elevations of 2024 PT₅ to calculate air mass range (Air Mass) are also referred to NASA JPL Horizons. Seeing FWHM (Seeing) in the r band for Seimei observations and in the Y, J, H, and K bands for Keck observations measured by computing the FWHM of reference stars are also listed.

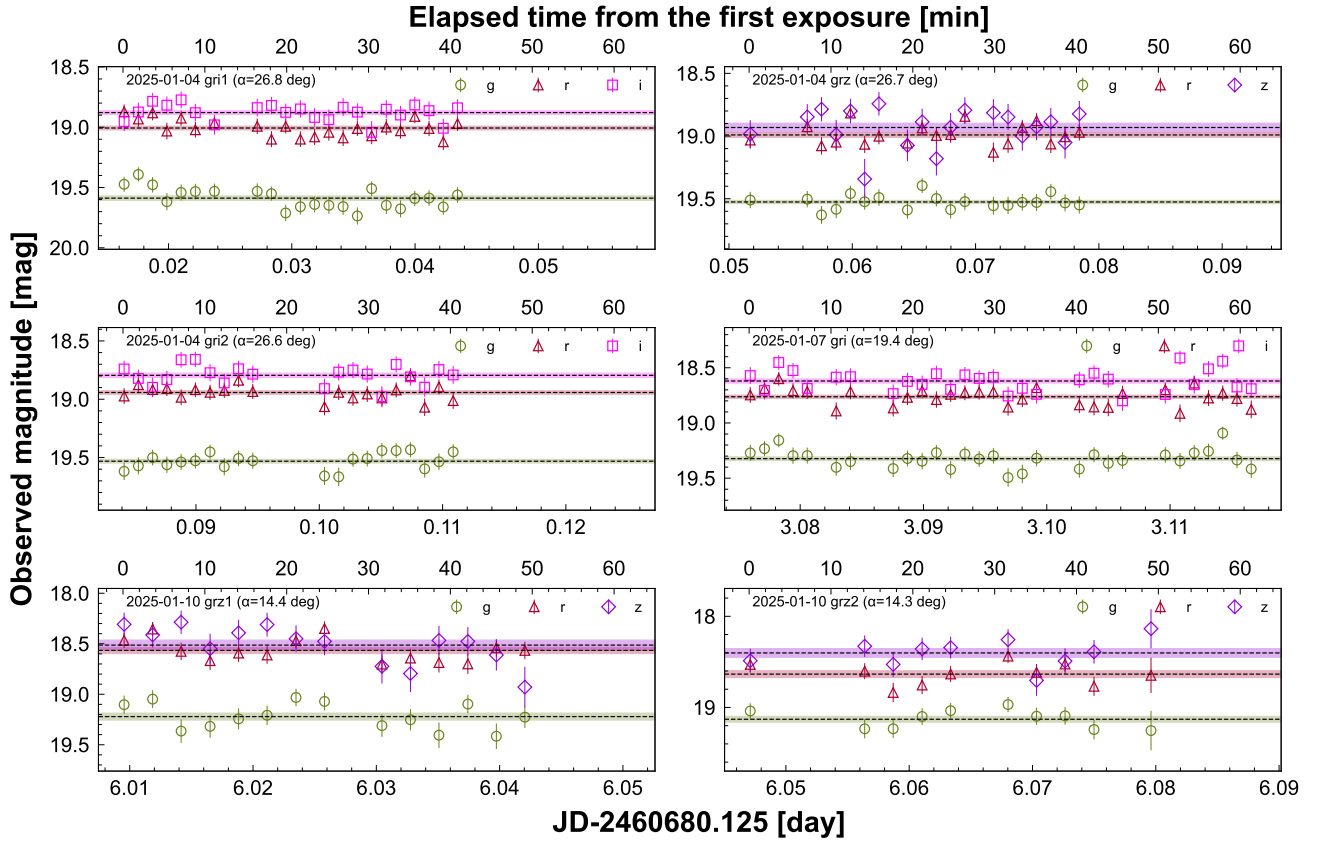


Fig. 4: Lightcurves of 2024 PT₅. The observed g , r , i , and z bands magnitudes are presented as circles, triangles, squares, and diamonds, respectively. Bars indicate the 1σ uncertainties. The arithmetic average of magnitude in each light curve is presented with a dashed line. Shaded areas indicate the standard errors of the averaged magnitudes.

are assigned for each asteroid. We extracted asteroids with 80% or higher probabilities to belong to a specific complex except U, which indicates an unknown class. We calculated $g-r$, $r-i$, and $r-z$ in the SDSS system, and then converted these colors into the Pan-STARRS system using equations given in Tonry et al.

(2012). By a visual inspection, 2024 PT₅ is overlapping with S-complex asteroids and lunar samples in the color-color diagrams.

We presented the derived near-infrared colors of 2024 PT₅ in Fig. 8. We also plotted near-infrared colors of NEAs from the literature: S-type (433) Eros (Chapman & Morrison 1976), S-type (25143) Itokawa (Ishiguro et al. 2003), S-type (1862) Apollo

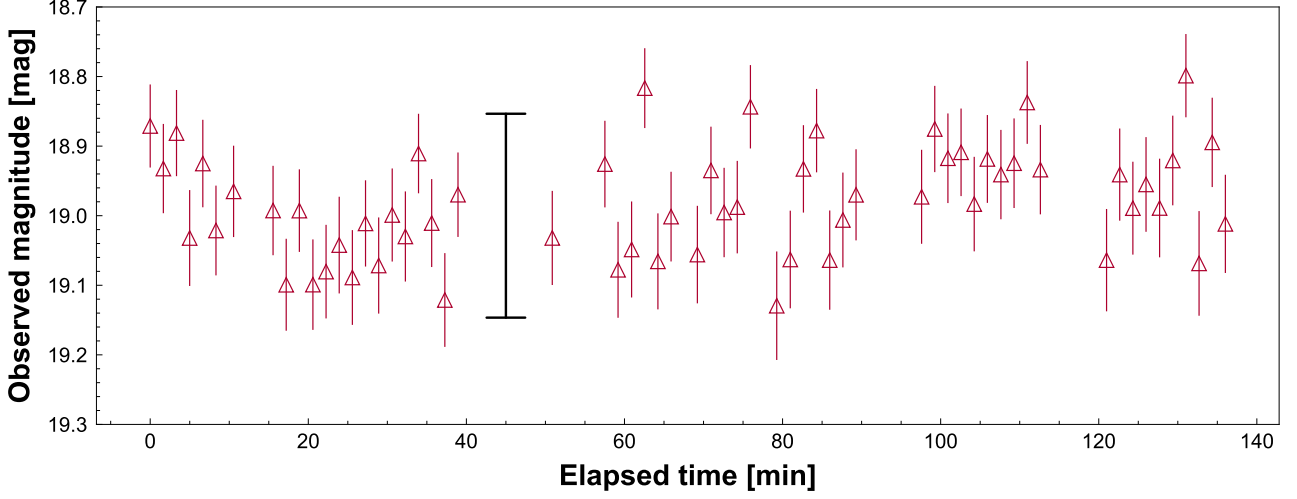


Fig. 5: Lightcurves of 2024 PT₅ in the r-band on January 4. Bars indicate the 1σ uncertainties. The variation of lightcurve, 0.3 mag, is indicated.

Table 3: Colors in the Pan-STARRS system

Objects	Reference	$g - r$	$r - i$	$r - z$
2024 PT ₅	Bolin et al. (2025a)	0.483 ± 0.043	0.286 ± 0.043	0.007 ± 0.059
	Kareta et al. (2025)	0.618 ± 0.029	0.205 ± 0.043	0.064 ± 0.083
	This study	0.567 ± 0.044	0.155 ± 0.009	0.147 ± 0.066
Kamo'oalewa	Sharkey et al. (2021)	0.47 ± 0.04	0.20 ± 0.04	0.25 ± 0.07
Lunar rock core samples	Isaacson et al. (2011)	0.48 ± 0.01	0.24 ± 0.04	0.14 ± 0.11

Notes. Colors of 2024 PT₅ in the SDSS system reported in Bolin et al. (2025a) were converted to those in the Pan-STARRS system using the equations in Tonry et al. (2012).

and C-type (4015) Wilson-Harrington (Hartmann et al. 1982), X-type 1012TC₄ (Urakawa et al. 2019; Reddy et al. 2019), and L-type (367943) Duende (de León et al. 2013; Takahashi et al. 2014). Solar system small bodies are serendipitously observed by survey observations in the near-infrared using 4.1 m Visible and Infrared Survey Telescope for Astronomy (VISTA) at ESO's Cerro Paranal Observatory, Chile. Infrared colors of minor bodies are extracted in Popescu et al. (2016, 2018). We presented the infrared colors of S, C, and X-type asteroids in Fig. 8 for comparison. We computed the $Y-J$, $Y-H$, and $J-H$ colors using the Y , J , and H observations from 2025 Jan 16. We compute the $Y-K_s$ color of 2024 PT₅ using the Y and K_s observations from 2025 Jan 17. The near-infrared colors of 2024 PT₅ are comparable to those of a Q-type asteroid Apollo and lunar samples, and $J-H$ color is redder than those of S-types, Eros, and Itokawa. The $Y-J$ color of 2024 PT₅ is estimated to be $Y - J = 0.557 \pm 0.046$. To compute the $H-K_s$ color of 2024 PT₅, we subtract the $Y-H$ color of 2024 PT₅ based on the Y and H observations taken on 2025 Jan 16 from the $Y-K_s$ color obtained from the Y and K_s observations 2025 Jan 17. The near-infrared color of 2024 PT₅ is similar to that of small S-complex NEA 2024 YR₄, measured with the same instruments (Bolin et al. 2025b), and consistent with its $J-H$ and $H-K_s$ colors. However, we identified possible systematics in the $Y-J$ color, likely caused by differences between the MOSFIRE and Pan-STARRS Y -band filter response functions. Therefore, we exclude the $Y-J$ color of 2024 PT₅ in the subsequent analysis.

3.3. Phase curve

We observed 2024 PT₅ across a wide phase angle range, from 14.3 deg to 26.8 deg. The Pan-STARRS magnitudes in the g and r bands were converted to Johnson V -band magnitudes using the following transformation provided by Tonry et al. (2012):

$$V = r + 0.006 + 0.474(g - r). \quad (6)$$

The phase curves of 2024 PT₅ in the V -band are shown in Fig. 9.

Since our phase curve lacks observations at lower phase angles, where opposition surges appear, we fitted it with simple models. We derived an absolute magnitude and slope of the phase curve with the linear model:

$$H_V(\alpha) = H_{V,\text{linear}} + b\alpha, \quad (7)$$

where $H_{V,\text{linear}}$ is an absolute magnitude in the V -band and b is the slope of the fitting curve. We also derived an absolute magnitude and slope of the phase curve with the $H-G$ model (Bowell et al. 1989):

$$H_V(\alpha) = H_{V,HG} - 2.5 \log_{10} ((1 - G)\Phi_1(\alpha) + G\Phi_2(\alpha)), \quad (8)$$

where $H_{V,HG}$ is an absolute magnitude in the V -band and G is the slope of the fitting curve. Φ_1 and Φ_2 are phase functions written

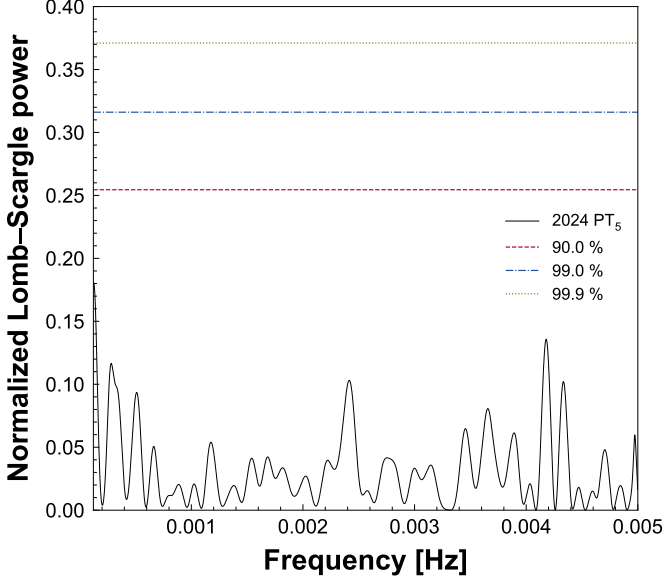


Fig. 6: Lomb–Scargle periodogram of 2024 PT₅. The number of harmonics of the model curve is unity. Dashed, dot-dashed, and dotted horizontal lines show 90.0, 99.0, and 99.9% confidence levels, respectively.

as follows with a basic function W :

$$\Phi_1(\alpha) = W \left(1 - \frac{0.986 \sin \alpha}{0.119 + 1.341 \sin \alpha - 0.754 \sin^2 \alpha} \right) + (1 - W) \exp \left(-3.332 \tan^{0.631} \frac{\alpha}{2} \right), \quad (9)$$

$$\Phi_2(\alpha) = W \left(1 - \frac{0.238 \sin \alpha}{0.119 + 1.341 \sin \alpha - 0.754 \sin^2 \alpha} \right) + (1 - W) \exp \left(-1.862 \tan^{1.218} \frac{\alpha}{2} \right), \quad (10)$$

$$W = \exp \left(-90.56 \tan^2 \frac{\alpha}{2} \right). \quad (11)$$

The uncertainties of $H_{V,\text{linear}}$, b , $H_{V,HG}$, and G were estimated with the Monte Carlo technique. We made 3000 phase curves by randomly resampling the data by assuming each observed datum follows a normal distribution whose standard deviation is the standard error of the error-weighted average magnitude. We derived fitting parameters as follows: $H_{V,\text{linear}} = 28.06 \pm 0.05$, $b = 0.029 \pm 0.002 \text{ mag deg}^{-1}$, $H_{V,HG} = 27.72 \pm 0.09$, and $G = 0.223 \pm 0.073$.

The Minor Planet Center (MPC) database contains 410 observations of 2024 PT₅ obtained from 44 different observatories. Of these, 404 observations include reported magnitudes. We used this dataset to estimate the phase curve of 2024 PT₅. To merge the heterogeneous data into a single reference photometric system, we collected observations of various asteroids from the MPC that were obtained using the same observatories and filters. We then computed the differences between the reported and predicted V magnitudes for these reference asteroids. The predicted V magnitudes were obtained using the Miriade software. These differences were used to correct the reported magnitudes of 2024 PT₅ to build a consistent dataset as shown in Fig. 10.

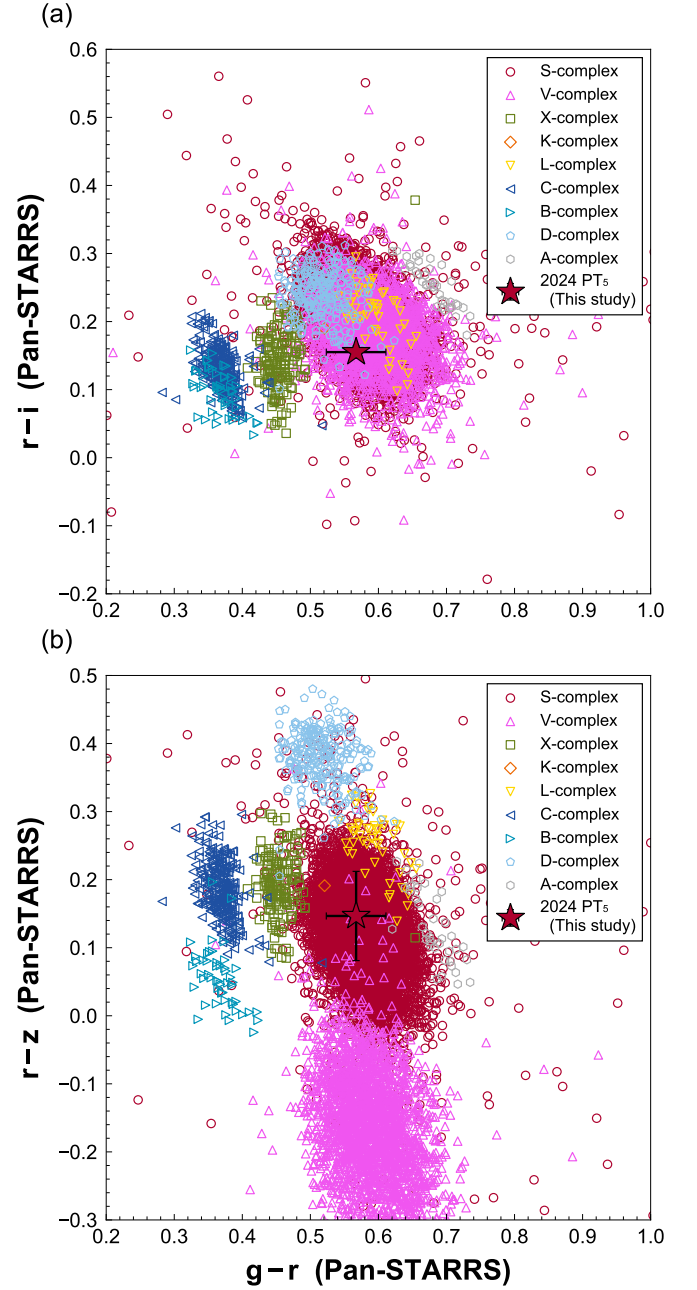


Fig. 7: Color-color diagram of (a) $g-r$ vs. $r-i$ and (b) $g-r$ vs. $r-z$. Mean of the individual nightly mean colors of 2024 PT₅ are plotted with stars. Error bars indicate the standard deviation of nightly mean colors. Error bars indicate the 1σ uncertainties. Asteroids from (Sergeyev & Carry 2021) are also plotted: S-complex (circles), V-complex (triangles), X-complex (squares), K-complex (diamonds), L-complex (inverse triangles), C-complex (left-pointing triangles), B-complex (right-pointing triangles), D-complex (pentagons), and A-complex (hexagons).

The fitting yielded the following parameters: $H_{V,\text{linear}} = 28.05 \pm 0.05$, $b = 0.029 \pm 0.001 \text{ mag deg}^{-1}$, $H_{V,HG} = 27.78 \pm 0.14$, and $G = 0.28 \pm 0.08$. The uncertainties in the parameters are given by the 1σ calculated as the square roots of the diagonal elements of the covariance matrix. These values are consistent

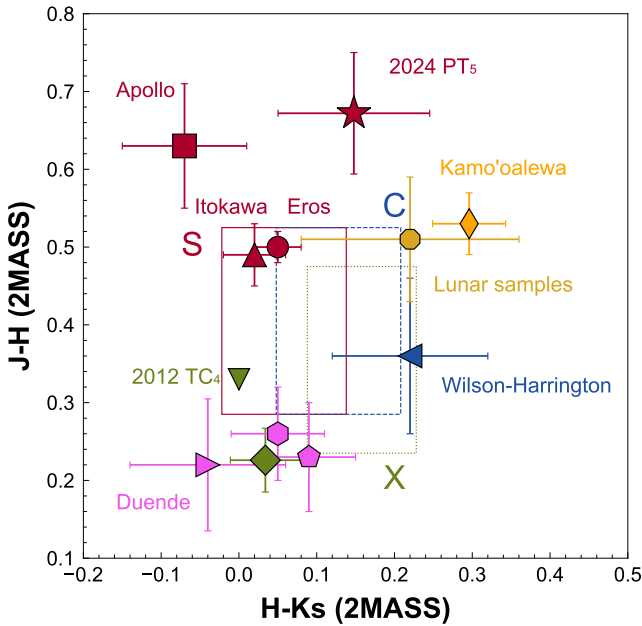


Fig. 8: Color-color diagram of $J-H$ vs. $J-K_s$. Colors of 2024 PT₅ are plotted with a star. Colors of near-Earth asteroids in the literature are plotted: Eros (circle) (Chapman & Morrison 1976), Itokawa (triangle) (Ishiguro et al. 2003), Apollo (square) (Hartmann et al. 1982), 2012 TC₄ (diamond and inverse triangle) (Urakawa et al. 2019; Reddy et al. 2019), Wilson-Harrington (left-pointing triangle) (Hartmann et al. 1982), and Duende (right-pointing triangle and pentagon) (de León et al. 2013; Takahashi et al. 2014). Error bars indicate the 1σ uncertainties. Average near-infrared colors of S-, C-, and X-types observed by VISTA-VHS are also indicated with rectangles (Popescu et al. 2016). Colors of lunar rock core samples (Isaacson et al. 2011) and Kamo'oalewa (Sharkey et al. 2021) are also shown by octagon and elongated diamond, respectively. The error bars correspond to the uncertainties of 1σ envelope of the compiled spectra in Fig. 12.

with those derived from our own measurements, however, the associated uncertainties are larger. Therefore, we adopt the parameters obtained solely from our measurements in the following discussion. We note that our computation is based on only three points, while the MPC data includes 404 points. Nevertheless, the results are very similar, and the consistency in results confirms the reliability of our values.

4. Discussion

4.1. Physical properties

The rotation state of 2024 PT₅ is still not clear, even with our lightcurves throughout more than 2 hr. The possibility that these variations are due to noise cannot be excluded. However, all published lightcurves, including ours, exhibit variations with a period of several tens of minutes. This indicates a tumbling motion of 2024 PT₅, as noted in previous studies (Kareta et al. 2025; de la Fuente Marcos et al. 2025). The fact that 2024 PT₅ is a tumbling asteroid supports the lunar ejecta origin since tumbling motion is expected after the collisional event (Harris 1994). We note that the tidal force can change the rotation state of 2024 PT₅

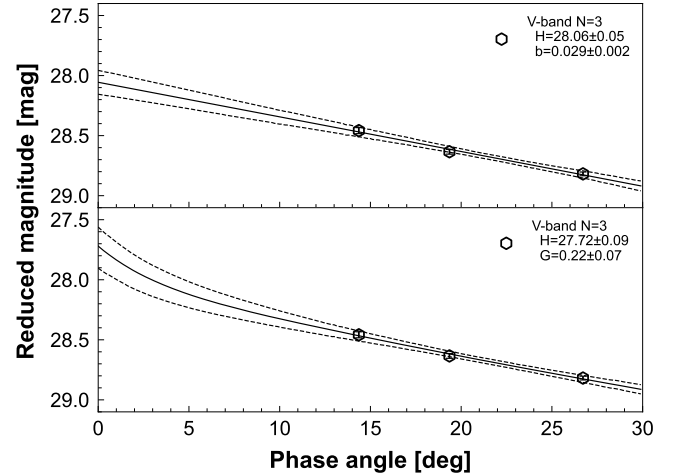


Fig. 9: Phase angle dependence of reduced V magnitudes of 2024 PT₅. Bars indicate the 1σ uncertainties. All magnitudes obtained on the same day are averaged and plotted. (top) The medians (50th percentile) of fitting model curves with the linear model are presented as solid lines. (bottom) The medians (50th percentile) of fitting model curves with the $H-G$ model are presented as solid lines. Uncertainty envelopes representing the 95% highest density interval values are shown by dashed lines.

during the close approach, as is reported for another tiny NEA (367943) Duende (a.k.a. 2012 DA₁₄, Moskovitz et al. 2020; Benson et al. 2020). 2024 PT₅ experienced a close approach with a distance of 0.00379 au or 1.5 Lunar distances (LD) from the Earth on 2024 August 8. The close encounter on 2024 August 8 and/or earlier close encounters may have changed the spin state of 2024 PT₅ inducing a tumbling state. This effect will be well studied for (99942) Apophis in 2029 during its ~ 0.07 LD close approach (Ballouz et al. 2024).

The derived visible colors of 2024 PT₅ in Table 3 and Fig. 7 are largely consistent with previous measurements by Bolin et al. (2025a) and Kareta et al. (2025), but with some differences of about 0.1 mag at most. This can be qualitatively explained when 2024 PT₅'s surface is not homogeneous within the uncertainties of measurements. Since our observation geometry was dramatically different from other studies as shown in Fig. 11, we might observe a different side of 2024 PT₅ compared to observations in 2024. However, qualitatively it is unrealistic to detect a change in colors of about 0.1 mag unless roughly half of the 2024 PT₅'s surface would have significantly different composition compared to the other half. A possible explanation is that 2024 PT₅ is tumbling, and the derived colors in previous observations are affected by the complex brightness variations. The simultaneous multicolor photometry we performed is a reliable method, unaffected by a possible complex rotation of 2024 PT₅ and less affected by observational artifacts.

As in the case of the rotation state, we note that close encounters with planets can change the surface properties, exposing fresh unweathered surface grains (e.g., Binzel et al. 2010). Very recently, however, McGraw et al. (2024) observed 2024 MK, a S-complex NEA like 2024 PT₅, before and after its close approach of 0.76 LD from the Earth. They obtained multiple high-quality visible to near-infrared spectra of 2024 MK using IRTF/SpEx on Mauna Kea. They found no planetary-encounter-induced spectral changes in the close approach, in contrast to previous works (e.g., Binzel et al. 2010), and concluded that a single close en-

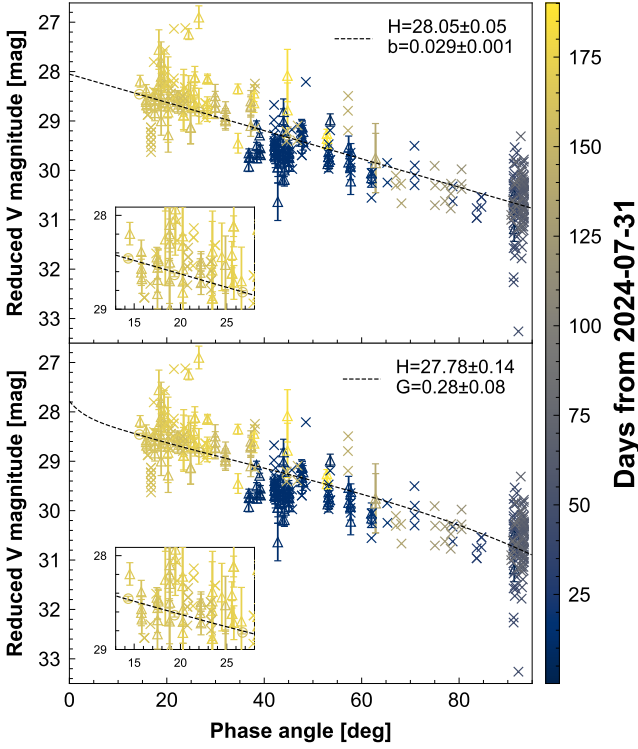


Fig. 10: Phase angle dependence of reduced V-band magnitudes of 2024 PT₅, including corrected observations from the MPC database. (top) Magnitudes obtained on the same day from Seimei/TriCCS are averaged and plotted by circles. Data from the MPC database with reported magnitude uncertainties are shown as triangles, while those without reported uncertainties are represented by crosses. Bars indicate the 1σ uncertainties. The fitting model curve with the linear model is presented as a dashed line. Each data point is color-coded by the observation date, expressed as days since 2024 July 31. The figure includes an inset plot that magnifies a region including data from Seimei/TriCCS. (bottom) Same as the top panel, but the data are fitted with the H - G model.

counter at 0.76 LD may not be enough to cause a detectable change in ground-based observations. As in the case of 2024 MK in McGraw et al. (2024), the phase reddening effect is also negligible for 2024 PT₅ since our observations are performed at phase angles less than 26.8 deg.

The b parameter derived in Sect. 3.3 has a tight correlation with geometric albedo (Belskaya & Shevchenko 2000):

$$b = C_1 - C_2 \log_{10} p_V, \quad (12)$$

where C_1 and C_2 are parameters obtained with phase slopes of asteroids whose albedo is estimated from thermal infrared observations. We used updated parameters $C_1 = 0.016 \pm 0.001$ and $C_2 = 0.022 \pm 0.001$ from Shevchenko et al. (2021). High-albedo asteroids have a shallower slope (smaller b) in the phase curves since the contribution of shadowing decreases as albedo increases (Belskaya & Shevchenko 2000). For instance, Shevchenko et al. (2012) estimated $b = 0.040$ – 0.045 mag deg⁻¹ for low-albedo Jupiter Trojans, Ishiguro et al. (2014) estimated $b = 0.039 \pm 0.001$ mag deg⁻¹ for low-

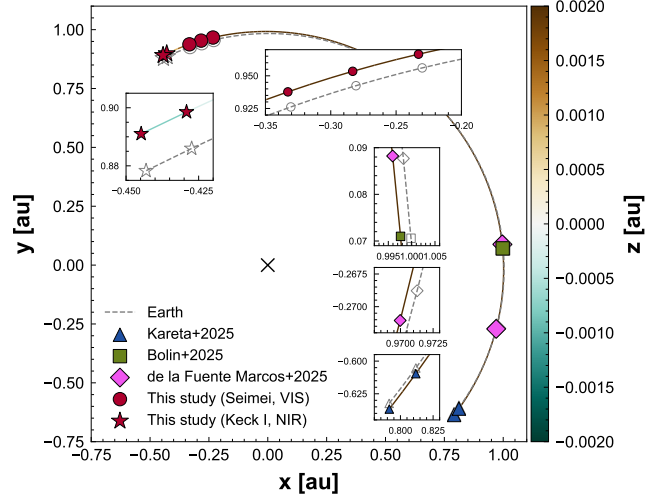


Fig. 11: Heliocentric positions of 2024 PT₅ and Earth at the time of observations in Kareta et al. (2025), Bolin et al. (2025a), de la Fuente Marcos et al. (2025), and this study. Positions of 2024 PT₅ and Earth are indicated by filled markers and open markers, respectively. Orbits of 2024 PT₅ and Earth are shown by solid and dashed lines, respectively. The color of the solid line indicates the z -coordinate (vertical position) of 2024 PT₅ in the heliocentric frame. The figure includes multiple inset plots that magnify specific regions. Although their scales differ, the aspect ratio is kept constant.

albedo NEA (162173) Ryugu, and Reddy et al. (2015) estimated $b = 0.0225 \pm 0.0006$ mag deg⁻¹ for high-albedo V-type NEA (357439) 2004 BL₈₆.

We derived a geometric albedo of 2024 PT₅ as 0.26 ± 0.07 with b_V derived from only our measurements. This is a fairly good match to S-type ($p_V = 0.24^{+0.04}_{-0.05}$) and Q-type ($p_V = 0.25^{+0.07}_{-0.04}$) NEAs (Marsset et al. 2022). This is confirmed from our G_V of 0.223 ± 0.073 , which is consistent with a typical value for S-types (Warner et al. 2009). The diameter of 2024 PT₅ can be estimated with our updated $H_{V,HG}$ and p_V using the following equation (Fowler & Chillemi 1992; Pravec & Harris 2007):

$$D = \frac{1329}{\sqrt{p_V}} \times 10^{-H_{V,HG}/5}. \quad (13)$$

The diameter of 2024 PT₅ is estimated to be 7.4 ± 1.0 m, which is consistent with the previous estimates, 5.4 ± 1.2 m (Bolin et al. 2025a) and $8 \leq D \leq 12$ m (Kareta et al. 2025).

A caveat is that it is unclear if we can apply the empirical relationship of Eq. 12 to such a tiny asteroid. The empirical relation in Belskaya & Shevchenko (2000); Shevchenko et al. (2021) is based on the WISE and AKARI measurements of relatively large asteroids, and it may not apply to tiny asteroids like 2024 PT₅ if their surface properties are different from those of large asteroids. Hasselmann et al. (2024) reported an unusual photometric phase curve of the NASA DART mission (Rivkin et al. 2021; Daly et al. 2023) and the ESA HERA mission (Michel et al. 2022) target S-type NEA (65803) Didymos ($D \sim 800$ m). They intensively analyzed the photometric phase curve of Didymos obtained at a wide range of phase angles, focusing not only on the linear slope but also on the opposition effect. They concluded that the photometric phase curve parameters are similar to those of M-type or C-complex asteroids, depending on the model used. To quantitatively estimate albedo,

cross validations by thermal infrared observations and/or polarimetry are important (e.g., Selmi et al. 2025). As for Didymos, it is expected that the Hera mission might end the discussion related to its surface properties. The Hayabusa2 extended mission (Hirabayashi et al. 2021) and Tianwen-2 mission (Zhang et al. 2021) will also enhance our understanding of two fast-rotating tiny NEAs, 1998 KY₂₆ ($D \leq 40$ m) and Kamo'oalewa ($D \leq 100$ m), respectively.

4.2. Origin of 2024 PT₅

Previous studies showed that the reflectance spectra of 2024 PT₅ match those of the lunar samples (Bolin et al. 2025a; Kareta et al. 2025; de la Fuente Marcos et al. 2025). Bolin et al. (2025a) concluded that the physical properties of 2024 PT₅ are compatible with an inner Main Belt or lunar ejecta with a preference to the latter, while both Kareta et al. (2025) and de la Fuente Marcos et al. (2025) concluded that their reflectance spectra are suggestive of a lunar origin. Their arguments are based on the similarity of reflectance spectra. de la Fuente Marcos et al. (2025) compared their visible to near-infrared (0.475 μ m to 0.880 μ m) reflectance spectrum of 2024 PT₅ with template spectra from DeMeo et al. (2009), and showed that the best-matching template is Sv-type, while they compared the spectrum of 2024 PT₅ with over 15000 spectra of meteorites, terrestrial rocks, and lunar soils in the RELAB database (Pieters 1983) using the M4AST tool (Popescu et al. 2012). Similarly, Kareta et al. (2025) compared their visible to near-infrared (~ 0.40 μ m to 2.45 μ m) reflectance spectrum of 2024 PT₅ with template spectra from DeMeo et al. (2009), and concluded that no taxonomic class fits the spectrum of 2024 PT₅. They compared the spectrum of 2024 PT₅ with every sample in the RELAB database.

The reflectance spectra of 2024 PT₅ in Fig. 12 were calculated with the derived and solar colors in the same manner as Beniyama et al. (2023b,a). For g , r , i , and z measurements, The reflectances at the central wavelength of the g , V , r , i , z , J , H , and K_s bands, R_g , R_V , R_r , R_i , R_z , R_J , R_H and R_{K_s} , were calculated as:

$$R_x = 10^{-0.4[(x-y)_{PT_5} - (x-y)_\odot]}, \quad (14)$$

where x and y are the indices of the bands. The reflectance at x -band is normalized relative to that of the y -band. $(x-y)_{PT_5}$ is the color of 2024 PT₅, and $(x-y)_\odot$ is the color of the Sun. We referred to the absolute magnitude of the Sun in the AB system as $g = 5.03$, $r = 4.64$, $i = 4.52$, and $z = 4.51$, and in the Vega system as $V = 4.81$, $J = 3.67$, $H = 3.32$, and $K_s = 3.27$ (Willmer 2018).

Using the seven band measurements in the visible to near-infrared, we tried to assess our 2024 PT₅'s spectrum. However, we cannot naturally connect our spectrum's visible and near-infrared portions. This could be due to the difference in observing geometries between Seimei/TriCCS and Keck/MOSFIRE observations as shown in Fig. 11; the cross section of the asteroid might have changed after Seimei/TriCCS observations owing to the changing aspect angle (Kwiatkowski & Kryszczyńska 1992; Jackson et al. 2022; Carry et al. 2024). Thus, we consider the visible and near-infrared measurements separately. We normalized reflectance spectra to unity at the V (0.5511 μ m) and J bands (1.2393 μ m) (Willmer 2018) in the visible and near-infrared wavelength portions of our spectrum as seen in the left and right panels of Fig. 12. Our visible spectra derived from colors are consistent with results of spectrophotometry in Bolin

et al. (2025a) and Kareta et al. (2025)⁵ as well as visible spectra shown in Kareta et al. (2025) and de la Fuente Marcos et al. (2025).

In Fig. 12, Mahlke templates of S- and A-type asteroids (Mahlke et al. 2022), a spectrum of Kamo'oalewa (Sharkey et al. 2021), and lunar rock core samples (Isaacson et al. 2011) are shown for comparison. The envelopes of lunar rock core samples are provided by Isaacson et al. (2011) by taking the average of lunar samples. In visible wavelengths, our spectrum matches well with both asteroids, such as S- and A-types templates, and lunar rock core samples. In the near-infrared wavelengths, the closest match is to lunar rock samples. These findings are consistent with previous studies (Bolin et al. 2025a; Kareta et al. 2025; de la Fuente Marcos et al. 2025). When considered separately, our reflectance spectrum is almost identical to that of Kamo'oalewa in visible and near-infrared wavelengths. However, the combined spectrum is less red than that of Kamo'oalewa, as reported in Kareta et al. (2025).

The orbital evolution of 2024 PT₅ before 1937 cannot be reconstructed due to a close encounter with Earth that causes orbital divergence (Kareta et al. 2025; de la Fuente Marcos et al. 2025). Therefore, to investigate the origin of 2024 PT₅ in terms of a dynamical point of view, we need to compare the likelihood of lunar ejecta origin and NEO population origin. Fedorets et al. (2020b) explored the lunar ejecta origin of the minimoons 2020 CD₃ by estimating the likelihood based on examining the contemporary production rate of small craters on the Moon with plausible assumptions regarding their properties (e.g., ejecta/impactor diameter ratio, ejecta speed). They ruled out a lunar ejecta origin for 2020 CD₃, and concluded that minimoons capture from the NEO population (Granvik et al. 2012; Fedorets et al. 2017) is a dominant mechanism for maintaining the minimoons steady-state population.

Recently, Jedicke et al. (2025) assessed the likelihood of both NEA origin (Granvik et al. 2012; Fedorets et al. 2017) and lunar ejecta origin for mini-moons using the steady-state size frequency distribution (SFD). As they discussed in the paper, there is systematic uncertainty of at least a few orders of magnitude on their SFD of lunar ejecta, taking the crater scaling relation, ejecta SFD, and ejecta size-speed relation into account. Thus, due to the model's large uncertainties, we cannot conclude whether NEA origin or lunar origin is preferred.

We cannot conclude the origin of 2024 PT₅ with our current knowledge from the discussion above, even when spectral and dynamical evidence are considered together. This conclusion is also valid for the minimoons 2020 CD₃. The visible geometric albedo of the Moon was derived in previous studies (e.g., Table 4 of Warell 2004). The estimated bulk visible geometric albedo of the Moon is ~ 0.15 . The area ratio of lunar mare and highland regions is around 43 % and 57 %, and the albedo for mare and highland is ~ 0.1 and ~ 0.2 (Korokhin et al. 2007). If 2024 PT₅ is of lunar origin, 2024 PT₅ could have originated from a bright highland region, as Kamo'oalewa could be from the lunar Gerdano Bruno crater (Jiao et al. 2024). The preference of the highland region is consistent with the argument from band center analysis in Kareta et al. (2025).

The Rubin Observatory Legacy Survey of Space and Time in Chile (LSST, Ivezić et al. 2019) is expected to observe more than five million asteroids, including 100,000 NEAs during its ten-year survey (Schwamb et al. 2023; Bolin et al. 2025c). Since there may be at least one minimoon of 1 m diameter (not of lu-

⁵ Downloaded from the Mission Accessible Near-Earth Objects Survey (MANOS) website, <https://manos.lowell.edu/>.

nar ejecta origin, but from NEO population) at any given time (Granvik et al. 2012), the LSST is expected to discover minimoons as well (Bolin et al. 2014; Fedorets et al. 2020a). The preparations for follow-up observation of future minimoon objects is thus highly encouraged, especially in both visible and near-infrared wavelengths are preferable as discussed in Kareta et al. (2025).

5. Conclusions

We conducted visible to near-infrared multicolor photometry of 2024 PT₅ with Seimei/TriCCS and Keck/MOSFIRE in January 2025. We derive color indices for 2024 PT₅ of $g-r = 0.567 \pm 0.044$, $r-i = 0.155 \pm 0.009$, $r-z = 0.147 \pm 0.066$, $Y-J = 0.557 \pm 0.046$, $J-H = 0.672 \pm 0.078$, and $H-K_s = 0.148 \pm 0.098$, which indicate that 2024 PT₅ is a typical S-type asteroid. Our three-days lightcurves are indicative of a tumbling motion of 2024 PT₅. A geometric albedo for 2024 PT₅ of 0.26 ± 0.07 was derived from the slope of its photometric phase curve, which is a fairly good match to S-type and Q-type NEAs. The albedo of 2024 PT₅ has not been previously reported. Using the $H-G$ model, we derived an absolute magnitude H_V of 27.72 ± 0.09 and a slope parameter G_V of 0.223 ± 0.073 in V-band. The diameter of 2024 PT₅ is estimated to be 7.4 ± 1.0 using the albedo and absolute magnitude. Based on the physical properties described above, our results are broadly consistent with a lunar spectral type, with similarity to other co-orbitals with lunar-like spectra such as 2020 CD₃ and Kamo'oalewa, and in agreement with existing works (Bolin et al. 2025a; Kareta et al. 2025; de la Fuente Marcos et al. 2025). This study shows that multiple observations at a wide range of phase angles using a medium-class telescope are essential to further investigate the origin of the minimoon 2024 PT₅.

Acknowledgements. We would like to thank Dr. Alessandro Morbidelli for insightful discussions and helpful comments. We thank Dr. Katsuhiro Murata for observing assistance using Seimei telescope. The authors are grateful to our reviewer Dr. Marcel Popescu for constructive comments on the manuscript. We acknowledge Dr. Robert Jedicke and Luis Langermann for the discussion regarding the steady state population of Earth's minimoons of lunar provenance and albedo of the Moon, respectively. J.B. thanks Dr. Theodore Kareta and Dr. Benjamin N. L. Sharkey for their constructive feedback on the spectra of 2024 PT₅ and Kamo'oalewa, respectively. J.B. is grateful to Dr. Max Mahlke for the development of, and valuable comments on, classy, a tool for exploring, downloading, analyzing, and classifying asteroid reflectance spectra. This work was supported by JSPS KAKENHI Grant Numbers JP23KJ0640 and 25H00665. This work was supported by the French government through the France 2030 investment plan managed by the National Research Agency (ANR), as part of the Initiative of Excellence Université Côte d'Azur under reference number ANR-15-IDEX-01. Some of the data presented herein were obtained at Keck Observatory, which is a private 501(c)3 non-profit organization operated as a scientific partnership among the California Institute of Technology, the University of California, and the National Aeronautics and Space Administration. The Observatory was made possible by the generous financial support of the W. M. Keck Foundation. Keck Observatory is located on Maunakea, land of the Kānaka Maoli people, and a mountain of considerable cultural, natural, and ecological significance to the indigenous Hawaiian people. The authors wish to acknowledge the importance and reverence of Maunakea and express gratitude for the opportunity to conduct observations from the mountain. This research has made use of LTE's Miriade VO tool.

References

Ballouz, R. L., Agrusa, H., Barnouin, O. S., et al. 2024, *PSJ*, 5, 251
 Belskaya, I. N. & Shevchenko, V. G. 2000, *Icarus*, 147, 94
 Beniyama, J., Ohsawa, R., Avdellidou, C., et al. 2023a, *AJ*, 166, 229
 Beniyama, J., Sako, S., Ohtsuka, K., et al. 2023b, *ApJ*, 955, 143
 Beniyama, J., Sekiguchi, T., Kuroda, D., et al. 2023c, *PASJ*, 75, 297
 Beniyama, J., Sergeyev, A. V., Tholen, D. J., & Micheli, M. 2024, *A&A*, 690, A180

Benson, C. J., Scheeres, D. J., & Moskovitz, N. A. 2020, *Icarus*, 340, 113518
 Binzel, R. P., Morbidelli, A., Merouane, S., et al. 2010, *Nature*, 463, 331
 Bolin, B., Jedicke, R., Granvik, M., et al. 2014, *Icarus*, 241, 280
 Bolin, B. T., Ahumada, T., van Dokkum, P., et al. 2022, *MNRAS*, 517, L49
 Bolin, B. T., Denneau, L., Abron, L.-M., et al. 2025a, *ApJ*, 978, L37
 Bolin, B. T., Fernandez, Y. R., Lisse, C. M., et al. 2021, *AJ*, 161, 116
 Bolin, B. T., Fremling, C., Holt, T. R., et al. 2020, *ApJ*, 900, L45
 Bolin, B. T., Hanuš, J., Denneau, L., et al. 2025b, *ApJ*, 984, L25
 Bolin, B. T., Masci, F. J., Coughlin, M. W., et al. 2025c, *Icarus*, 425, 116333
 Bowell, E., Hapke, B., Domingue, D., et al. 1989, in *Asteroids II*, ed. R. P. Binzel, T. Gehrels, & M. S. Matthews (Tucson, AZ: Univ. Arizona Press), 524–556
 Carry, B., Peloton, J., Le Montagner, R., Mahlke, M., & Berthier, J. 2024, *A&A*, 687, A38
 Chambers, K. C., Magnier, E. A., Metcalfe, N., et al. 2016, *arXiv:1612.05560*, *arXiv:1612.05560*
 Chapman, C. R. & Morrison, D. 1976, *Icarus*, 28, 91
 Daly, R. T., Ernst, C. M., Barnouin, O. S., et al. 2023, *Nature*, 616, 443
 de la Fuente Marcos, C. & de la Fuente Marcos, R. 2018, *MNRAS*, 473, 2939
 de la Fuente Marcos, C. & de la Fuente Marcos, R. 2020, *MNRAS*, 494, 1089
 de la Fuente Marcos, R., de León, J., de la Fuente Marcos, C., et al. 2023, *A&A*, 670, L10
 de la Fuente Marcos, R., de León, J., Serra-Ricart, M., et al. 2025, *A&A*, 694, L5
 de León, J., Ortiz, J. L., Pinilla-Alonso, N., et al. 2013, *A&A*, 555, L2
 DeMeo, F. E., Binzel, R. P., Slivan, S. M., & Bus, S. J. 2009, *Icarus*, 202, 160
 Denneau, L., Robinson, J., Fitzsimmons, A., et al. 2024, *Minor Planet Electronic Circulars*, 2024-P170
 Fedorets, G., Granvik, M., & Jedicke, R. 2017, *Icarus*, 285, 83
 Fedorets, G., Granvik, M., Jones, R. L., Jurić, M., & Jedicke, R. 2020a, *Icarus*, 338, 113517
 Fedorets, G., Micheli, M., Jedicke, R., et al. 2020b, *AJ*, 160, 277
 Fowler, J. W. & Chillemi, J. R. 1992, *Phillips Lab. Tech. Rep.*, 2049, 17
 Ginsburg, A., Sipőcz, B. M., Brasseur, C. E., et al. 2019, *AJ*, 157, 98
 Gladman, B. J., Burns, J. A., Duncan, M. J., & Levison, H. F. 1995, *Icarus*, 118, 302
 Glass, I. S. 1999, *Handbook of Infrared Astronomy*
 Granvik, M., Jedicke, R., Bolin, B., Chyba, M., & Patterson, G. 2013, in *Asteroids: Prospective Energy and Material Resources*, ed. V. Badescu, 151–167
 Granvik, M., Vaubaillon, J., & Jedicke, R. 2012, *Icarus*, 218, 262
 Harris, A. W. 1994, *Icarus*, 107, 209
 Hartmann, W. K., Cruikshank, D. P., & Degewij, J. 1982, *Icarus*, 52, 377
 Hasselmann, P. H., Della Corte, V., Pravec, P., et al. 2024, *PSJ*, 5, 91
 Hirabayashi, M., Mimasu, Y., Sakatani, N., et al. 2021, *Advances in Space Research*, 68, 1533
 Isaacson, P. J., Pieters, C. M., Besse, S., et al. 2011, *Journal of Geophysical Research (Planets)*, 116, E00G11
 Ishiguro, M., Abe, M., Ohba, Y., et al. 2003, *PASJ*, 55, 691
 Ishiguro, M., Kuroda, D., Hasegawa, S., et al. 2014, *ApJ*, 792, 74
 Ivezić, Z., Kahn, S. M., Tyson, J. A., et al. 2019, *ApJ*, 873, 111
 Jackson, S. L., Rozitis, B., Dover, L. R., et al. 2022, *MNRAS*, 513, 3076
 Jedicke, R., Alessi, E. M., Wiedner, N., et al. 2025, *arXiv e-prints*, *arXiv:2504.17985*
 Jedicke, R., Bolin, B. T., Bottke, W. F., et al. 2018, *Frontiers in Astronomy and Space Sciences*, 5, 13
 Jiao, Y., Cheng, B., Huang, Y., et al. 2024, *Nature Astronomy*, 8, 819
 Kareta, T., Fuentes-Muñoz, O., Moskovitz, N., Farnocchia, D., & Sharkey, B. N. L. 2025, *ApJ*, 979, L8
 Kary, D. M. & Dones, L. 1996, *Icarus*, 121, 207
 Korokhin, V. V., Velikodsky, Y. I., Shkuratov, Y. G., & Mall, U. 2007, *Solar System Research*, 41, 19
 Kurita, M., Kino, M., Iwamuro, F., et al. 2020, *PASJ*, 72, 48
 Kwiatkowski, T. & Kryszczyńska, A. 1992, in *Liege International Astrophysical Colloquia*, Vol. 30, *Liege International Astrophysical Colloquia*, ed. A. Brahic, J. C. Gerard, & J. Surdej, 353
 Kwiatkowski, T., Kryszczyńska, A., Poliška, M., et al. 2009, *A&A*, 495, 967
 Lang, D., Hogg, D. W., Mierle, K., Blanton, M., & Roweis, S. 2010, *AJ*, 139, 1782
 Lomb, N. R. 1976, *Ap&SS*, 39, 447
 Mahlke, M., Carry, B., & Mattei, P. A. 2022, *A&A*, 665, A26
 Marsset, M., DeMeo, F. E., Burt, B., et al. 2022, *AJ*, 163, 165
 McCully, C., Crawford, S., Kovacs, G., et al. 2018, *Astropy/Astrocrappy: V1.0.5 Zenodo Release*, Zenodo
 McGraw, L. E., Thomas, C. A., Lister, T. A., et al. 2024, *ApJ*, 977, L25
 McLean, I. S., Steidel, C. C., Epps, H. W., et al. 2012, in *Society of Photo-Optical Instrumentation Engineers (SPIE) Conference Series*, Vol. 8446, *Ground-based and Airborne Instrumentation for Astronomy IV*, ed. I. S. McLean, S. K. Ramsay, & H. Takami, 84460J
 Michel, P., Küppers, M., Bagatin, A. C., et al. 2022, *PSJ*, 3, 160
 Mommert, M., Kelley, M., de Val-Borro, M., et al. 2019, *The Journal of Open Source Software*, 4, 1426

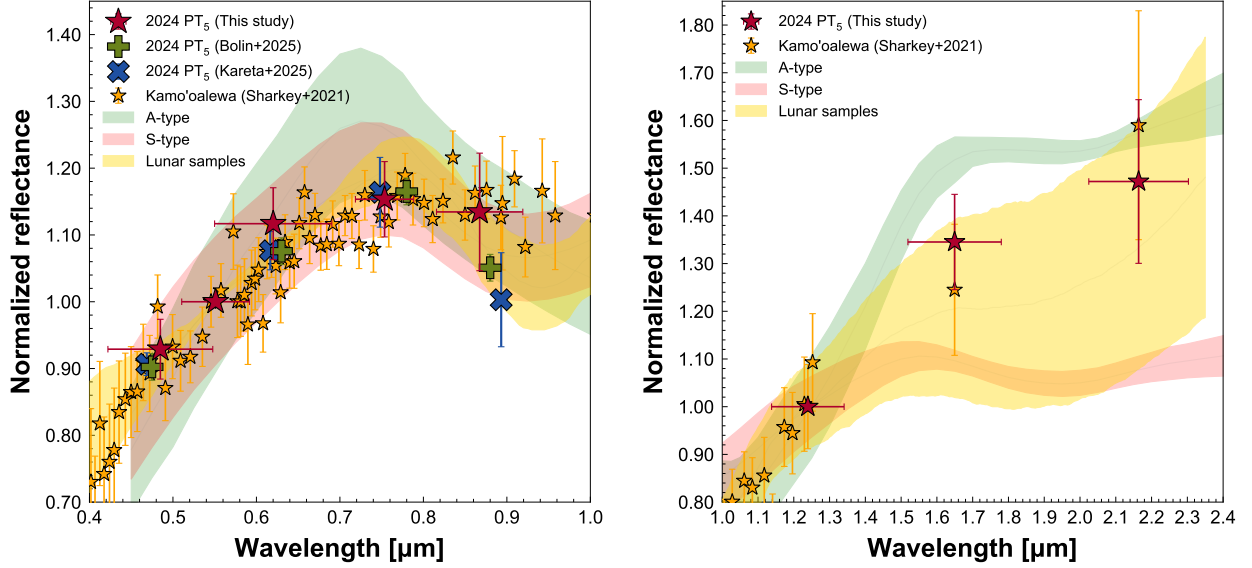


Fig. 12: Reflectance spectrum of 2024 PT₅ and Kamo'oalewa (Sharkey et al. 2021). Also, Mahlke templates of A- and S-type asteroids are shown (Mahlke et al. 2022). Shaded areas indicate the standard deviations of the template spectra. The lunar rock core sample colors are also shown (Isaacson et al. 2011). Shaded areas correspond to the 1σ envelope of the compiled spectra.

- Moskovitz, N. A., Benson, C. J., Scheeres, D., et al. 2020, *Icarus*, 340, 113519
 Naidu, S. P., Micheli, M., Farnocchia, D., et al. 2021, *ApJ*, 913, L6
 Pieters, C. M. 1983, *J. Geophys. Res.*, 88, 9534
 Popescu, M., Birlan, M., & Nedelcu, D. A. 2012, *A&A*, 544, A130
 Popescu, M., Licandro, J., Carvano, J. M., et al. 2018, *A&A*, 617, A12
 Popescu, M., Licandro, J., Morate, D., et al. 2016, *A&A*, 591, A115
 Pravec, P. & Harris, A. W. 2007, *Icarus*, 190, 250
 Reddy, V., Gary, B. L., Sanchez, J. A., et al. 2015, *ApJ*, 811, 65
 Reddy, V., Kelley, M. S., Farnocchia, D., et al. 2019, *Icarus*, 326, 133
 Rivkin, A. S., Chabot, N. L., Stickle, A. M., et al. 2021, *PSJ*, 2, 173
 Scargle, J. D. 1982, *ApJ*, 263, 835
 Schwamb, M. E., Jones, R. L., Yoachim, P., et al. 2023, *ApJS*, 266, 22
 Selmi, E., Devogèle, M., Masiero, J. R., et al. 2025, *PSJ*, 6, 26
 Sergeyev, A. V. & Carry, B. 2021, *A&A*, 652, A59
 Sharkey, B. N. L., Reddy, V., Malhotra, R., et al. 2021, *Communications Earth and Environment*, 2, 231
 Shevchenko, V. G., Belskaya, I. N., Slyusarev, I. G., et al. 2012, *Icarus*, 217, 202
 Shevchenko, V. G., Mikhalechenko, O. I., Belskaya, I. N., et al. 2021, *Planet. Space Sci.*, 202, 105248
 Skrutskie, M. F., Cutri, R. M., Stiening, R., et al. 2006, *AJ*, 131, 1163
 Takahashi, J., Urakawa, S., Terai, T., et al. 2014, *PASJ*, 66, 53
 Tonry, J. L., Stubbs, C. W., Lykke, K. R., et al. 2012, *ApJ*, 750, 99
 Urakawa, S., Ohsawa, R., Sako, S., et al. 2019, *AJ*, 157, 155
 van Dokkum, P. G. 2001, *PASP*, 113, 1420
 VanderPlas, J. T. 2018, *ApJS*, 236, 16
 Warell, J. 2004, *Icarus*, 167, 271
 Warner, B. D., Harris, A. W., & Pravec, P. 2009, *Icarus*, 202, 134
 Willmer, C. N. A. 2018, *ApJS*, 236, 47
 Zappala, V., Cellino, A., Barucci, A. M., Fulchignoni, M., & Lupishko, D. F. 1990, *A&A*, 231, 548
 Zhang, T., Xu, K., & Ding, X. 2021, *Nature Astronomy*, 5, 730